RESEARCH PAPER

Micro-meso-macroscale correlation mechanism of red-bed soft rocks failure within static water based on energy analysis

Zhen Liu[1,2] · Jin Liao[1,2] · Chang Xia[1,2] · Cuiying Zhou[1,2] · Lihai Zhang[3]

Abstract

The purpose of the present study is to fundamentally investigate the micro-meso-macroscale correlation mechanism of red-bed soft rocks failure within static water, based on energy analysis. Through a series of experimental studies, changes in the micro-meso-macroscale characteristics of the rocks were characterised by measuring ion concentrations in and pH of water, the pore structure and crack propagation. Based on the experimental measurements, theoretical modelling of micro-meso-macroscale energy conservation was carried out to determine the micro-meso-macroscale correlation mechanism of red-bed soft rocks failure. The results show that the microscale dominant effect of red-bed soft rocks is determined as chemical effects. The failure mechanism of red-bed soft rocks under static water saturation involves chemical, physical and mechanical dominant effects at the micro-meso-macroscale. It was demonstrated that the dominant chemical effect of clay minerals and water comprises a series of chemical energy changes in the microscale water–rock interface. This can induce the energy changes in both mesophysical and macromechanical levels. During the first month after the water saturation, there was a significant decrease in Na^+ and K^+ concentrations in aqueous solution, whereas there was little change in Ca^+ and Mg^{2+} concentrations. The scanning electron microscope (SEM) images indicated an obvious change in microstructure of the red-bed soft rocks after 3 months of water saturation. A decrease in pore number and increase in total pore surface area could be seen after 6 months of water saturation. Furthermore, the theoretical results suggest that chemical effects at the microscale dominate the softening process of the rocks. During the water–rock interaction, nearly 80% of the energy dissipation results from the microscale change, and the meso-macroscale change accounts for the remaining 20%. As a uniform measure of material evolution, energy can correlate the micro-meso-macro dominant effect of red-bed soft rocks softening appropriately.

Keywords Energy conservation · Micro-meso-macroscale correlation · Pore structure · Red-bed soft rocks · Static water saturation · SEM imaging

List of symbols

ΔH	Enthalpy change
Q_{micro}	Microscale energy
Q_{meso}	Mesoscale energy
Q_{macro}	Macroscale energy
Q_{total}	Total scale energy
Q_{sum}	Total scale energy subtract overlapping energy
$Q_{conservation}$	Theoretical modelling of energy conservation under water–rock interaction
$Q_{overlap}$	Overlapping energy of meso and macro
Q_1	Adsorption energy
Q_2	Chemical energy
n	Molar amount of adsorbed ions in solution
E_a	Unit molar adsorption energy
c_i	The molar concentration of i-th reaction
$V_{r/w}$	Volume of sample or volume of aqueous solution
$\triangle_r H_m{}^0{}_i$	Standard molar enthalpy change of i-th reaction
E_b	Energy of added surface area after softening and disintegration of red-bed soft rocks

✉ Cuiying Zhou
zhoucy@mail.sysu.edu.cn

1   School of Civil Engineering, Sun Yat-sen University, No.135 XinGangXiLu, Guangzhou 510275, China

2   Guangdong Engineering Research Centre for Major Infrastructure Safety, Guangzhou 510275, China

3   Department of Infrastructure Engineering, The University of Melbourne, Melbourne, VIC 3010, Australia

G_{1c}	Energy per unit surface of red-bed soft rocks	$\triangle T_{rock}$	Temperature change of red-bed soft rocks
$A_{surface}$	Newly increased surface area of red-bed soft rocks	$\triangle T_{water}$	Temperature change of water
$A_{particle}$	Surface area of particles	c_{rock}	Specific heat capacity of silty mudstone
Q_v	Swelling energy	c_{water}	Specific heat capacity of water
V_1 and V_2	Volumes before and after swelling	E_1	Elastic modulus of red-bed soft rocks
P	Swelling stress	α	Coefficient of thermal expansion
V	Volume of red-bed soft rocks	ε	Thermal expansion strain
W_e	Elastic property of soft rocks with volume V_v	d	Particle diameter of red-bed soft rocks
μ	Poisson's ratio of red-bed soft rocks	e	Sum of porosity and volume change rate
E	Elastic modulus of red-bed soft rocks		
W_1	Fracture energy caused by crack		
W_2	Fracture energy caused by voids		
W_f	Energy dissipated due to initial crack slip		
U_e	Energy dissipated due to tensile crack propagation		
W_V	Fracture energy of voids when pore volume is V_{matrix}		
$2c$	Initial crack length		
$2l$	Tensile crack length		
$2w$	Distance between adjacent cracks		
θ	Angle between initial crack surface and axial stress		
τ_f	Shear force produced by the external load sliding on initial crack surface		
τ^*	Shear force produced by the external load sliding on tensile crack surface		
v	Friction coefficient between crack surfaces		
E	Elastic modulus		
k	A constant, in plane stress state		
σ_{eq}	Equivalent stress		
ε_{eq}^p	Equivalent plastic strain		
U^s	Work on shear stress		
U^f	Work on friction		
U^c	Work for complete cutting on convex surface		
U^n	Work for normal load		
U^η	Work on viscous drag		
V_{fluid}	Fluid velocity		
A	Frictional surface area		
l_i	Frictional distance		
U^c	Work when the concave convex part is completely sheared during process of shearing		
U_p	Frictional energy of particles		
F_s	Frictional force of collision friction between particles		
F_n	Average impact force on the indirect contact surface of particles		
$\triangle t$	Time of particle collision and friction		
V_{water}	Volume of water in container		
m_{sample}	Quality of red-bed soft rocks sample		
$\triangle H_{resultant}$	Standard molar enthalpy of resultant		
$\triangle H_{reactant}$	Standard molar enthalpy of reactant		

1 Introduction

Although red-bed soft rocks demonstrate good mechanical properties, a series of physical, chemical and mechanical effects can occur if the rocks contact water, which may lead to their mechanical failure. To date, the study on softening behaviour of soft rocks mainly focuses on the external representation and the correlation of macromechanics and mesophysical effects, while the research work on microscale mechanism of the rocks is not cohesive [1, 15, 22, 24, 38, 46, 70, 71, 73].

Previous experimental studies on the softening processes of the soft rocks have mainly focussed on the decomposition and transformation of a single type of mineral [20, 21, 40, 55], while the change in mesoparticles and pores in soft rocks was investigated using scanning electron microscope (SEM) and high-definition digital imaging [36, 37, 54, 69]. Although a series of mechanical tests of soft rocks (e.g. consolidated undrained and drained triaxial testing) have been carried out [14, 17, 27], mechanical testing with consideration of water effect needs to be further investigated. The relationship between the macroscale mechanical behaviour and mesoscale structure of soft rocks was experimentally studied using the combination of scanning electron microscope, computed tomography scanning, digital image correlation and advanced imaging techniques [31, 53, 66]. However, changes at the microscale of soft rocks due to chemical reactions under the action of water are not fully understood.

The current theoretical models on studying the deformation and failure mechanism of soft rocks based on fractal and energy dissipation theories have limited capabilities to determine the relationship between the mechanics and structure at mesoscale [47, 49, 61]. The plastic deformation stress model, continuous damage model, FLAC3D rheological constitutive model and anisotropic damage model of soft rocks were developed for investigating the relationship between macroscale and mesoscale dominant effects during

the softening process [4, 8, 13, 23, 72]. A series of saturated soft rocks models were developed based on, for example, the evolutionary neural network, renormalisation group theory, damage fractional theory, free entropy theory and viscoelastic plastic creep theory [25, 28, 74], but the physical–chemical interaction was not studied. A range of contact models, crack propagation models and damage evolution models were established to study the energy dissipation of rock failure [6, 50, 57]. However, it narrowly focuses on the transformation and dissipation of damage energy under deformation and failure such as elastic–plastic properties and surface energy under macroscale stress–strain strength. In short, the study of soft rocks softening is based on external representation and the correlation of macromechanics and mesophysical effects. Literature on the microscale mechanism is not cohesive. The process of energy balance change under the action of water and rock is deeply undiscussed.

The purpose of this study is to investigate the micro-meso-macroscale correlation mechanism of red-bed soft rocks failure within static water, based on energy, by conducting a series of experimental studies in conjunction with theoretical modelling. First, the dominant factors (ion concentrations in and pH of water, the pore structure and crack propagation) that govern changes in the micro-meso-macroscale characteristics of red-bed soft rocks were experimentally studied. The micro-meso-macroscale energy conservation and failure mechanism were then theoretically investigated.

2 Materials and method

Red-bed soft rocks samples obtained from Southern China were used for the experimental testing. Figure 1 shows the methodology in this study for establishing the micro-meso-macroscale correlationship of soft rocks under water–rock interaction.

2.1 Experimental studies

2.1.1 Preparation of red-bed soft rock samples

Typical silty mudstone samples were collected from Southern China. The main clay mineral content in the rock samples was kaolinite, illite and quartz. There was a small amount of sericite, chlorite, muscovite, montmorillonite and iron. The size of cylindrical silty mudstone samples is φ50 mm × 100 mm. The samples are tested by sound wave velocity, and the samples with large dispersion of sound wave velocity are eliminated. After extracting the defective samples, 15 samples were ultimately got (Fig. 2). The rock samples were placed into a plastic box (250 mm × 250 mm × 250 mm) containing water taken from the Dongjiang River basin, Southern China. The tops of the samples were 10 cm below the water surface. To prevent excessive water evaporation, the plastic box was fully covered.

The test conditions for the samples were (I) natural condition, (II) water saturation for 1 month, (III) water saturation for 3 months, (IV) water saturation for 6 months and (V) water saturation for 12 months. To reduce the uncertainty of experimental measurements, three samples were used for each of the tests, as shown in Table 1. The samples were described as I (1,2,3), II (1,2,3), III (1,2,3), IV (1,2,3) and V (1,2,3).

### 2.1.2 Measuring ion concentrations in and pH of water solution

The time-dependent change in ion concentrations (e.g. Na^+, Ca^{2+} etc.) in and pH of water solution for each test was measured using ion chromatograph (Model: Dionex ICS-900, Resolution: 0.05 mg/L) and pH reagent, respectively. Regularly take a small amount of rock blocks from the same point of soft rock samples. A small amount of rock blocks was ground into powder and passed through 0.5-mm sieve after naturally drying. The powder is packed in self-sealing bags and numbered. The time-dependent change in chemical components of rock samples under water saturation was studied using inductively coupled plasma emission spectrometer (Model: iCAP6500Duo, Resolution: 0.001 mg/L) in the Instrumental Analysis and Research Center, Sun Yat-sen University. Because of the massive difference in the magnitude of each chemical composition in soft rock, Fig. 5 is drawn by percentage as ordinate. To reduce the uncertainty of experimental measurements, the average value of the measurement data of 3 samples in each group is taken as a point of each test scene (Fig. 5 and Fig. 6). The purpose is to characterise the microbehaviour of red-bed soft rocks samples under static water action.

2.1.3 Measuring pore structure of rock samples

Regularly take a small amount of rock blocks from the same point of soft rock samples. A small amount of rock blocks was fixed on the sample table after freeze drying. Gold was sprayed on the surface of the rock blocks to improve the quality and resolution of the image. Then the time-dependent change in pore structure of rock samples under water saturation was studied using SEM (Model: Gemini 500, Resolution: 0.6 nm) in the Instrumental Analysis and Research Center, Sun Yat-sen University. The obtained SEM images were processed using the SEM Image Processing Tool. The mesobehaviour of the red-bed soft rocks samples under water action can be quantitatively characterised by SEM.
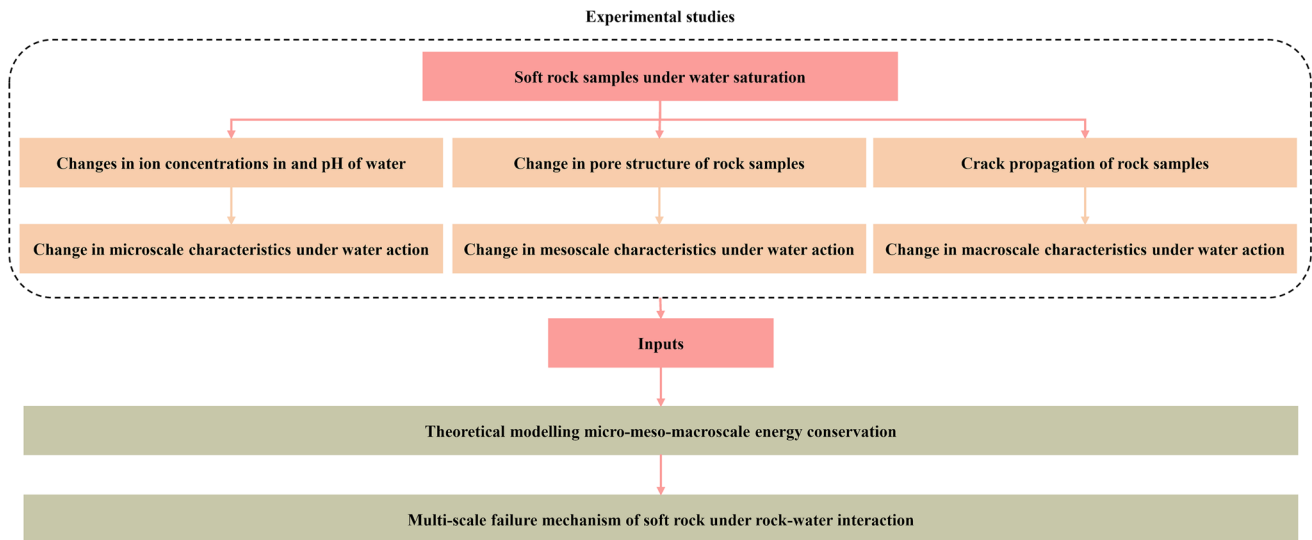
Fig. 1 Flow chart of experimental and theoretical methodology for investigating the failure mechanism of red-bed soft rocks under water–rock interaction
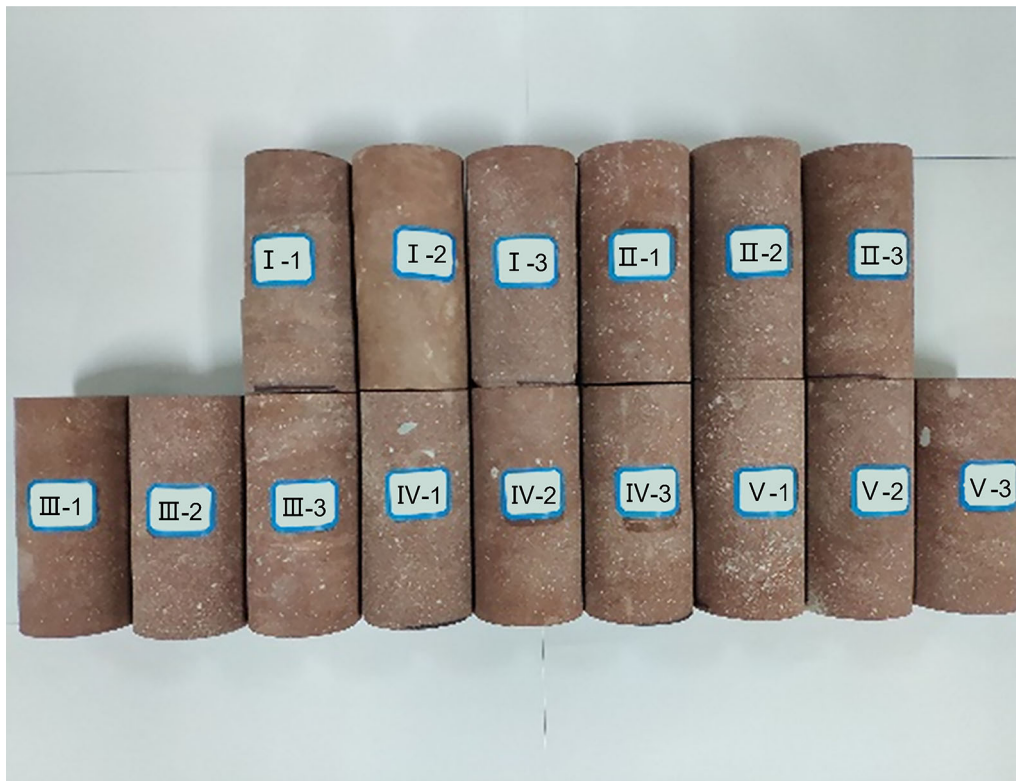
Fig. 2 Cylindrical silty mudstone samples

2.1.4 Monitoring crack propagation of rock samples

The crack propagation of rock samples resulting from steady-state water–rock interaction was monitored using visual inspection (high-speed camera), so that the macrobehaviour of rock samples could be characterised.

2.2 Theoretical modelling

The experimentally measured change in micro-meso-macrocharacteristics of red-bed soft rocks samples under water action was theoretically analysed by modelling enthalpy change based on energy conservation with the aim

Table 1 Test conditions for red-bed soft rock samples

Test number	Sample number	Test scenario
I	I-1	Natural condition
	I-2	
	I-3	
II	II-1	Water saturation for 1 month
	II-2	
	II-3	
III	III-1	Water saturation for 3 months
	III-2	
	III-3	
IV	IV-1	Water saturation for 6 months
	IV-2	
	IV-3	
V	V-1	Water saturation for 12 months
	V-2	
	V-3	

of establishing the relationship of micro-meso-macroscale changes in soft rocks characteristics under water action.

2.2.1 Modelling change in microscale characteristics of red-bed soft rocks under water action

Based on previous studies [66, 67, 70], the mesoscale dominant effect is a physical effect, and the macroscale dominant effect is a mechanical effect. On this basis, the microscale dominant effect can be determined.

The scale of red-bed soft rocks is divided mainly granting to the size of the selected objects in Physics (Fig. 3).

Microscale: it primarily studies the change process of functional groups, mineral grain structure, solution pH and ion concentration. The microeffects of rocks were analysed by microtests such as Fourier transform microinfrared spectrometer, ion chromatograph and pH reagent.

Mesoscale: it is reflected in mesodamage like dislocation friction between clay particles, volume expansion between particles, expansion and accumulation of pore cracks. It was observed by optical microscope or scanning electron microscope to study its mesoeffect.

Macroscale: it mainly includes mechanical damage, swelling, rock mass falling off and disintegration in the laboratory. The macroscale rock and soil mass are studied by indoor and field test equipment, and its deformation and mechanical properties are analysed.
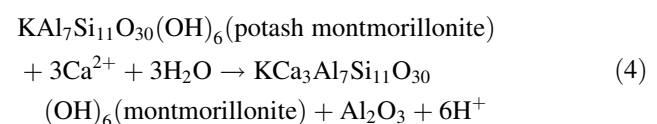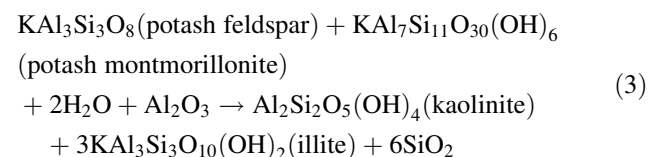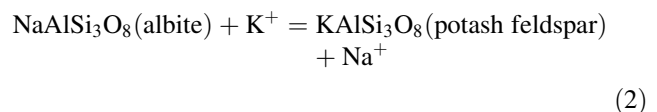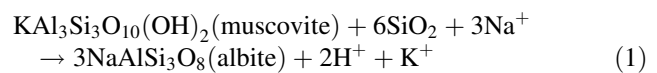
The mesoscale characteristics of the red-bed soft rocks can be described by physical characteristics of the rocks (e.g. pore structure), while the damage behaviour of the rocks (e.g. crack propagation) represents the macroscale

characteristics of the rocks. For the microscale characteristics of the red-bed soft rocks, the ion compositions in and pH of water resulting from water–rock interaction were investigated. The chemical behaviour at the microscale due to water–rock interaction could lead to the change in mechanical properties at macroscale and ultimately the failure of the rocks [56, 58, 64]. Therefore, it can be said that the chemical effect is the dominant effect at the microscale of red-bed soft rocks.

In conclusion, the microscale, mesoscale and macroscale catastrophic behaviour of red-bed soft rocks can be characterised by chemical effects, physical effects and mechanical effects, respectively.

As shown in Fig. 1, the present theoretical study on changes in the microscale characteristics of red-bed soft rocks under water saturation mainly focussed on the change in ion concentration and pH of water. Figure 4 shows that, at the water–rock interface, clay minerals, which are often negatively charged, attract cations in the aqueous solution, resulting in the formation of a hydration shell. The chemical reactions involving ion-exchange adsorption, dissolution and formation of soluble minerals lead to the production of water-soluble substances [38], resulting in the loss of element structure of the clay mineral layer.

Based on the previous studies and on time-dependent change in ion concentration in water during water–silty mudstone interaction under normal temperature and pressure conditions [5, 18, 33, 40, 44, 51, 52, 59], Considering the simplified calculation and the high concentration of Na^+ and Ca^{2+} ions in the solution, feldspar only considers the transformation of albite and potash feldspar. And Fig. 5 and Eqs. (1)–(6) describe the chemical transformation of muscovite, feldspar, montmorillonite, kaolinite, chlorite and illite involving Na^+, K^+ and Ca^{2+} ions in the solution and synthesised albite, potash feldspar and anorthite.

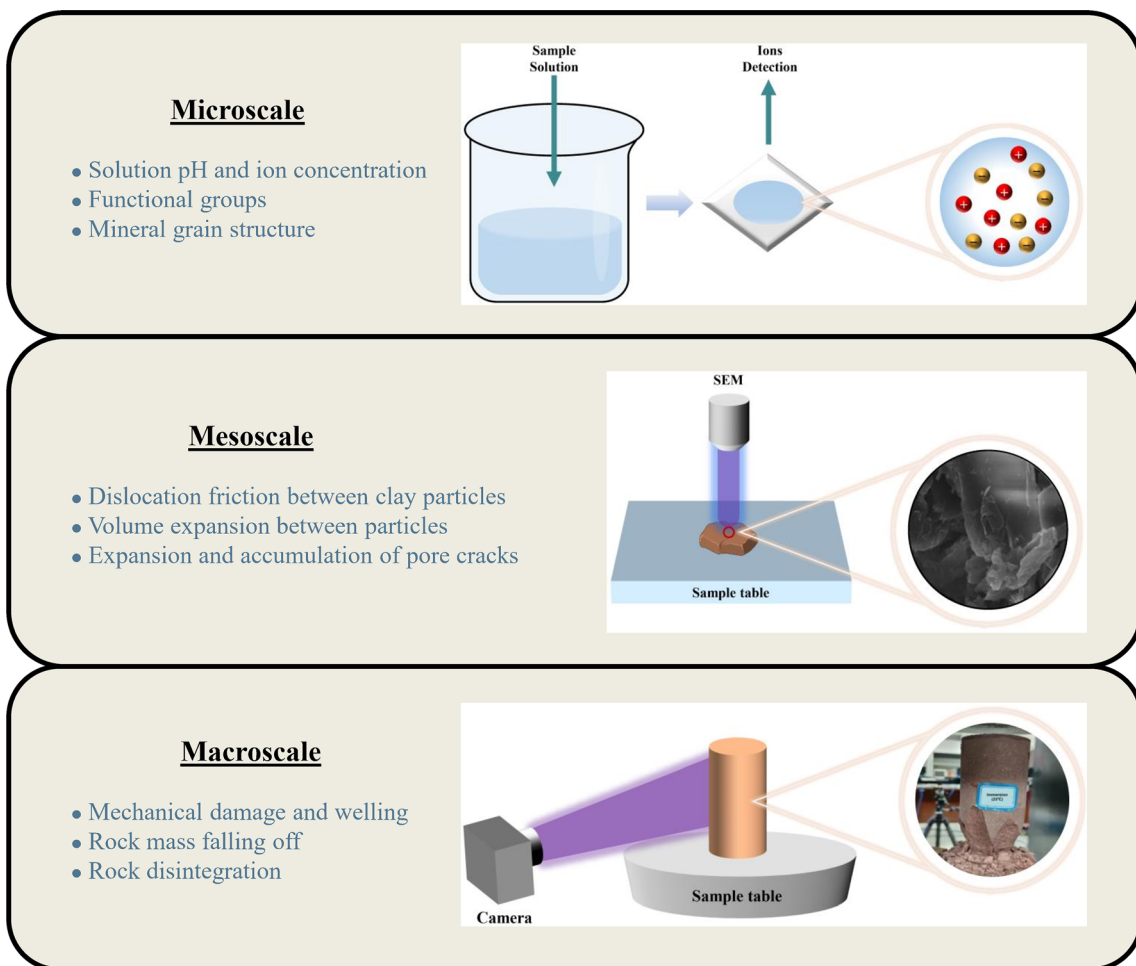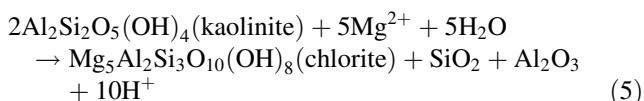$$KAl_3Si_3O_{10}(OH)_2(muscovite) + 6SiO_2 + 3Na^+ \rightarrow 3NaAlSi_3O_8(albite) + 2H^+ + K^+ \quad (1)$$

$$NaAlSi_3O_8(albite) + K^+ = KAlSi_3O_8(potash\ feldspar) + Na^+ \quad (2)$$

$$KAl_3Si_3O_8(potash\ feldspar) + KAl_7Si_{11}O_{30}(OH)_6$$
$$(potash\ montmorillonite)$$
$$+ 2H_2O + Al_2O_3 \rightarrow Al_2Si_2O_5(OH)_4(kaolinite)$$
$$+ 3KAl_3Si_3O_{10}(OH)_2(illite) + 6SiO_2 \quad (3)$$

$$KAl_7Si_{11}O_{30}(OH)_6(potash\ montmorillonite)$$
$$+ 3Ca^{2+} + 3H_2O \rightarrow KCa_3Al_7Si_{11}O_{30}$$
$$(OH)_6(montmorillonite) + Al_2O_3 + 6H^+ \quad (4)$$

Fig. 3 The scale of red-bed soft rocks

$$2Al_2Si_2O_5(OH)_4(\text{kaolinite}) + 5Mg^{2+} + 5H_2O$$
$$\rightarrow Mg_5Al_2Si_3O_{10}(OH)_8(\text{chlorite}) + SiO_2 + Al_2O_3$$
$$+ 10H^+ \quad (5)$$

$$K_2O + 5H_2O \rightarrow 2KOH \quad (6)$$

Chemical reaction involves energy absorption and release, which can be described by the change in enthalpy (ΔH). There is a heat absorption of red-bed soft rocks from water when $\Delta H > 0$, while the release of heat from the rocks into water happens when $\Delta H < 0$. Thus, ΔH can be used to characterise the microscale dissolution and formation of rock minerals. The microscale energy (Q_{micro}) can be divided into adsorption energy (Q_1) and chemical energy (Q_2) [70]. That is,

$$Q_{\text{micro}} = Q_1 + Q_2 = n \cdot E_a + \sum_{i=1}^{n} c_i \cdot V_{r/w} \cdot \Delta_r H_{m_i}^0 \quad (7)$$

where n is the molar amount of adsorbed ions in solution, E_a is the unit molar adsorption energy, c_i is the molar concentration of i-th reaction, $V_{r/w}$ is the volume of

aqueous solution, and $\Delta_r H_m{}^0{}_i$ is the standard molar enthalpy change of the i-th reaction.

2.2.2 Modelling change in mesoscale characteristics of red-bed soft rocks under water action

During the water–rock interaction process, the chemical behaviour of the red-bed soft rocks at the microscale results in pore structure at the mesoscale involving change in potential energy, swelling energy and other types of energy [70]. It is assumed that potential energy and swelling energy are 2 major types of energy at the mesoscale.

The potential energy caused by the increase of specific surface area due to the accumulation of microcracks and pores can be expressed as [32]

$$E_b = G_{1c} \cdot A_{\text{surface}} \quad (8)$$

where E_b is the change in energy in rock surface due to softening and disintegration of red-bed soft rocks, G_{1c} is the energy per unit rock surface, and A_{surface} is the newly
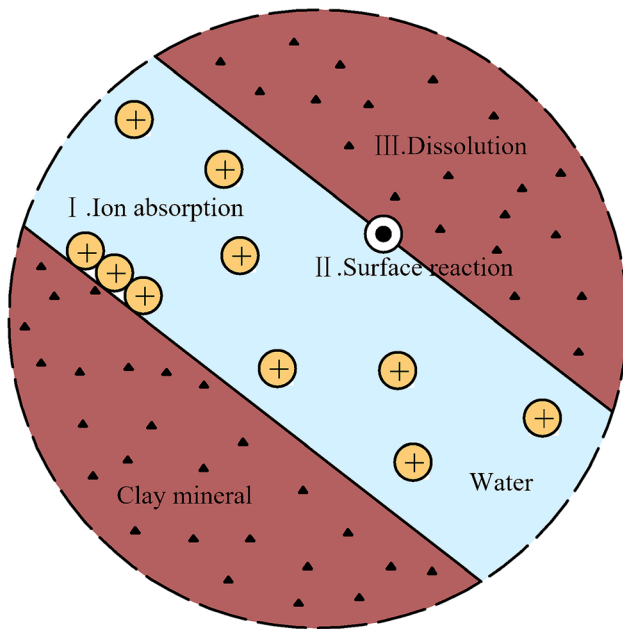
Fig. 4 Dissolution and diffusion diagram of clay minerals at water–rock interface

increased surface area of red-bed soft rocks. The swelling energy of mesoscale clay minerals can be expressed as [45]

$$Q_v = -\int_{V_1}^{V_2} P dV \tag{9}$$

where Q_v is the swelling energy, V_1 and V_2 are the volumes before and after swelling, respectively, P is the swelling stress, and V is the volume of red-bed soft rocks.

2.2.3 Modelling change in macroscale characteristics of red-bed soft rocks under water action

In this study, the study of macroscale energy of red-bed soft rocks mainly focuses on strain energy and frictional energy. Strain energy can be divided into elastic potential energy and plastic potential energy.

The elastic potential energy can be expressed as [60]

$$W_e = \left[\sigma_1^2 + \sigma_2^2 + \sigma_3^2 - 2\mu(\sigma_1\sigma_2 + \sigma_1\sigma_3 + \sigma_2\sigma_3)\right]/(2E) \cdot V_v \tag{10}$$

where W_e is the elastic property of red-bed soft rocks with a volume of V_v, μ is the Poisson's ratio of red-bed soft rocks, and E is the elastic modulus of red-bed soft rocks.

The plastic potential energy, which consists of crack-breaking energy and void-breaking energy, can be described as [12]

$$W_p = W_1 + W_2 = W_f + 2U_e + W_v = 2c\tau_f \frac{(k+1)(1+\mu)}{2E\sin\theta}$$
$$\cdot \left[\frac{2c\tau^*\sin\theta}{\sqrt{w\sin\frac{\pi(l+l^*)}{w}}} - \sigma_2\sqrt{2w\tan\frac{\pi l}{2w}} + \sigma_2\sqrt{\frac{\pi l}{2}}\right] \cdot \sqrt{2\pi(l+l^{**})}$$
$$+ \frac{(k+1)(1+\mu)}{E} \cdot \left[\frac{4c^2\tau^{*2}\sin^2\theta}{\pi}\ln\left[\frac{\tan\frac{\pi(l+l^*)}{2w}}{\tan\frac{\pi l^*}{2w}}\right]\right.$$
$$-4\sigma_2^2\frac{w^2}{\pi}\ln\left(\cos\frac{\pi l}{2w}\right) - 8c\tau^*\sigma_2\sin\theta\frac{w}{\pi} \cdot$$
$$\left.\ln\left[\tan\frac{\pi}{4}\left(1+\frac{l}{w}\right)\right]\right] + V_{matrix} \cdot \sigma_{eq} \cdot \varepsilon_{eq}^p \tag{11}$$

where W_1 is the fracture energy caused by cracking, W_2 is the fracture energy induced by the development of voids,
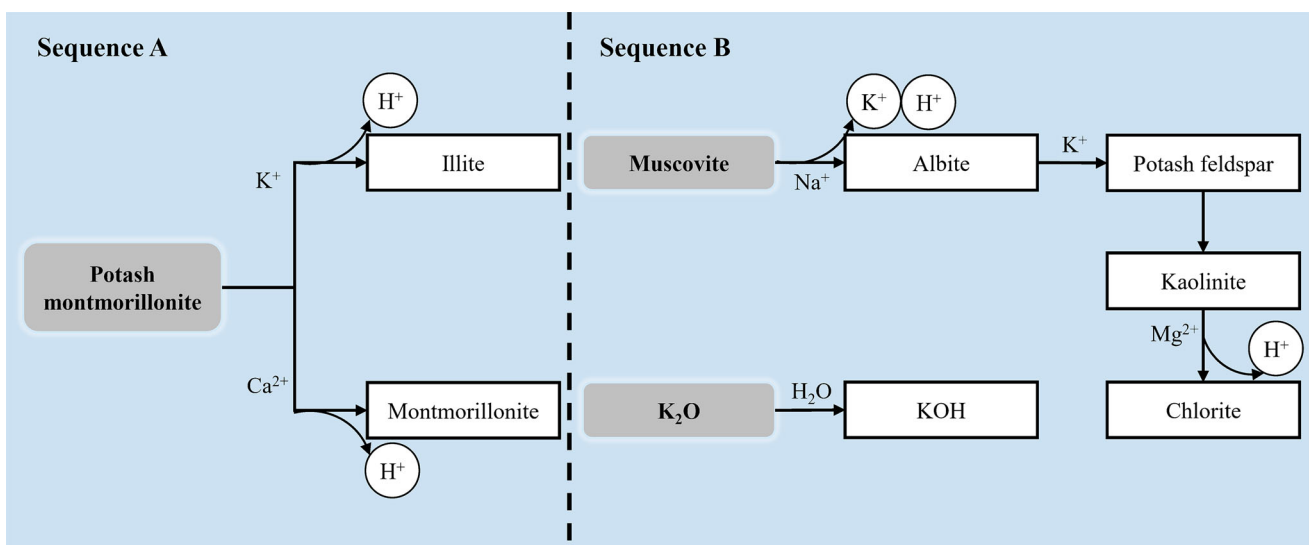
Fig. 5 Schematic diagram showing chemical reactions at water–rock interface

W_f is the energy dissipated due to initial slippage of cracks, U_e is the energy dissipated due to tensile crack propagation, W_V is the fracture energy of void development, and the pore volume is V_{matrix}. The initial crack length is $2c$ with a tensile crack length of $2\,l$ ($l^* \approx 0.27c$ and $l^{**} = 0.083c$). The distance between adjacent cracks is $2w$, and the angle between the initial crack surface and the axial stress is θ. τ_f is the shear force produced by the external load sliding on the initial crack surface $\left(\tau_f = \frac{1}{2}\mu[(\sigma_1 + \sigma_2)-(\sigma_1-\sigma_2)\cos 2\theta]\right)$. τ^* is the shear force produced by the external load sliding on the tensile crack surface $\left(\tau^* = \frac{1}{2}(\sigma_1-\sigma_2)\sin 2\theta - \frac{1}{2}v[(\sigma_1 + \sigma_2)-(\sigma_1-\sigma_2)\cos 2\theta]\right)$.

v is the friction coefficient between crack surfaces, E is the elastic modulus, and μ is the Poisson's ratio of the material. $k = (3-\mu)/(1 + \mu)$ is a constant in plane stress state. σ_{eq} is the equivalent stress, and ε_{eq}^{p} is the equivalent plastic strain. Since there is little change in elastic energy, it is reasonable to assume that $\varepsilon_{eq}^{p} = \varepsilon_{eq}$.

The macroscale frictional energy of red-bed soft rocks consists of the heat generated by the friction of structural plane and that generated by friction of particles. The adiation energy, kinetic energy and other types of energy are ignored in this study [16, 29, 48, 62, 63]. The frictional energy of the structural plane can be expressed as [2, 3, 30]

$$U^s = U^f + U^c + U^n + U^\eta \quad (12)$$

where U^s is work done by shear stress. $U^f = \sum\limits^{n} \tau_f A l_i$ is work done by friction, where A is the frictional surface area and l_i is the frictional distance. U^c is work done by complete cutting on convex surface and is ignored in this study by assuming a flat structure plan without concave convex fluctuation, in order to simplify the calculation. U^n is work done by normal load. For a flat surface, there is no difference in height between the undulating surface and the frictional surface (i.e. $h = 0$). Thus, $U^n = \sigma_n, h = 0$. U^η is the work done by resistance between red-bed soft rocks and fluid. Since $V_{fluid} = 0$, U^η can also be ignored.

The frictional energy of red-bed soft rocks particles (U_p) can be expressed as [65]

$$U_p = \frac{F_s \cdot F_n \cdot \Delta t^2}{m} \quad (13)$$

where $F_s = \tau_f$ is the frictional force of collision friction between particles and $F_n = mg$ is the average impact force on the indirect contact surface of particles. $\triangle t$ is the time of particle collision and friction (0.100 s), and m is the particle mass.

2.2.4 Modelling micro-meso-macroscale energy conservation of red-bed soft rocks under water action

The overall water–rock interaction can be modelled based on conservation of energy. According to the above analysis, the different types of energy caused by the crack propagation and change in pore structure can be expressed as

$$Q_{meso} + Q_{macro} = E_b + Q_v + W_e + W_p + E_v + U_s + U_p \quad (14)$$

where Q_{meso} is the change of energy due to mesoscale physical effects and Q_{macro} is the change of energy due to macroscale mechanical effects. Finally, the relationship between microscale adsorption energy and chemical energy is

$$\begin{aligned} Q_{total} &= Q_{micro} + Q_{meso} + Q_{macro} \\ &= Q_1 + Q_2 + E_b + Q_v + W_e + W_p + U_s + U_p \end{aligned} \quad (15)$$

where Q_1 is the adsorption energy, Q_2 is the chemical energy, E_b is the potential energy caused by the increase of surface area resulting from red-bed soft rocks softening and disintegrating, Q_v is the swelling energy of red-bed soft rocks, W_e is the elastic potential energy of red-bed soft rocks, W_p is the plastic potential energy of red-bed soft rocks, U_s is the structural plane frictional energy of red-bed soft rocks, and U_p is the frictional energy of mudstone particles.

At the microscale, ion adsorption and chemical reaction occurring at the water–rock interface lead to the swelling of fracture pores at the mesoscale and, ultimately, energy change resulting from the increase of specific surface area. Therefore, there is no overlap between microscale energy and mesoscale energy. For macroscale energy, the strain energy in the stress–strain curve overlaps with the potential energy in the mesoscale. That is,

$$Q_{overlap} = E_b \cap \left(W_e + W_p\right) = W_e + W_p \quad (16)$$

Thus, the energy conservation under water–rock interaction can be expressed as

$$\begin{aligned} Q_{conservation} &= Q_{micro} + Q_{meso} + Q_{macro} - Q_{overlap} + Q_{water} \\ &= Q_1 + Q_2 + E_b + Q_v + W_e + W_p + U_s + U_p \\ &= \Delta C \end{aligned} \quad (17)$$

where $Q_{conservation}$ is the energy conservation under water–rock interaction, and $Q_{overlap}$ is the overlapping energy at the mesoscale and macroscale. ΔC is a constant ($\Delta C = 0$ if there is no energy exchange with the outside).
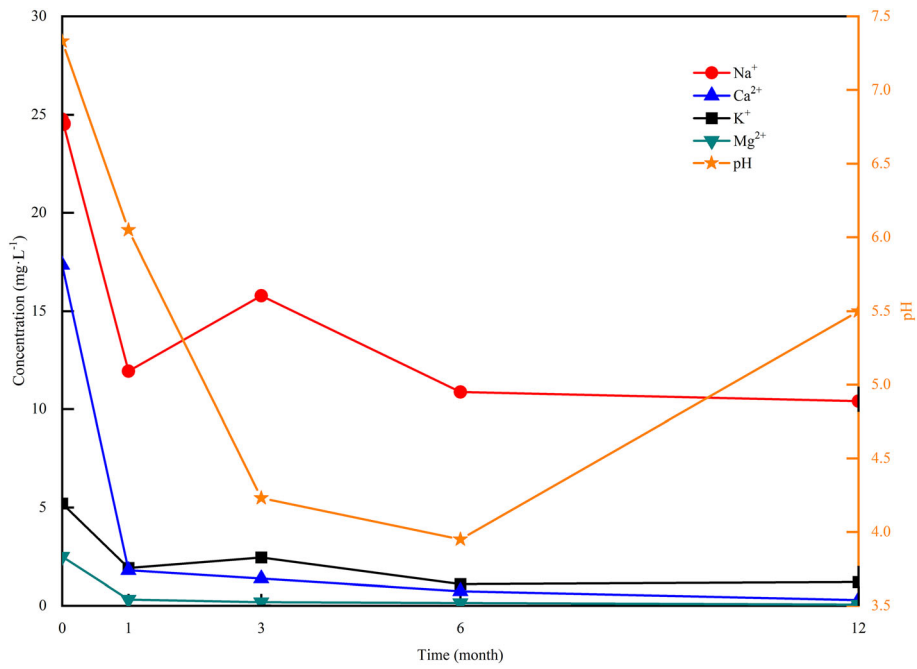
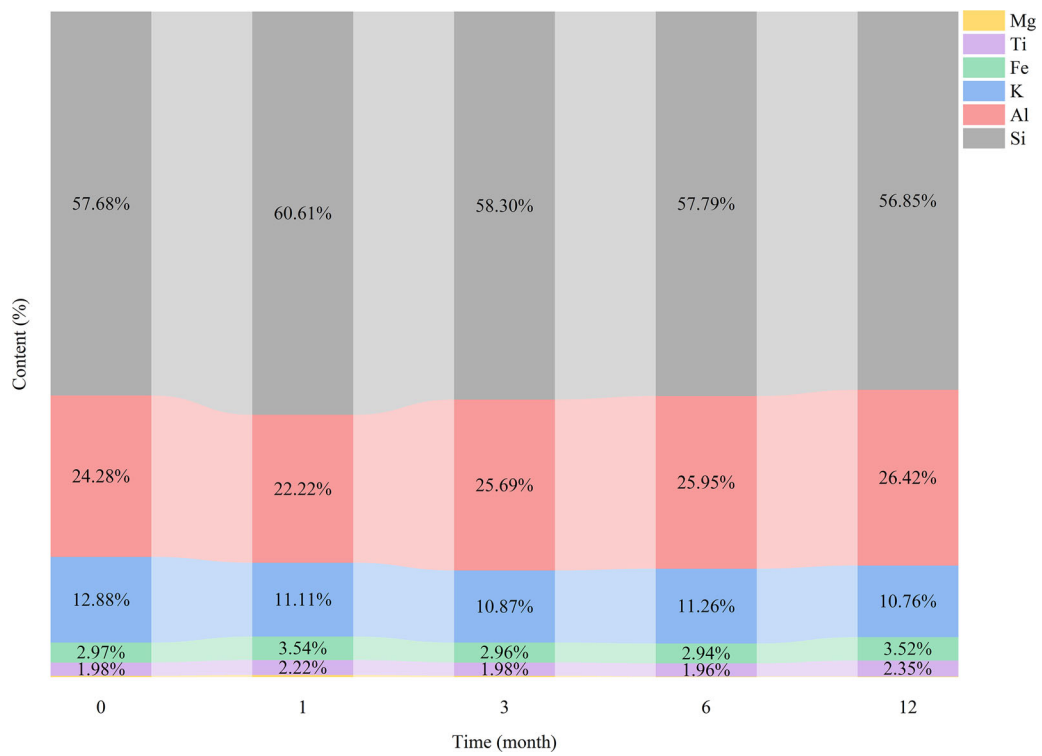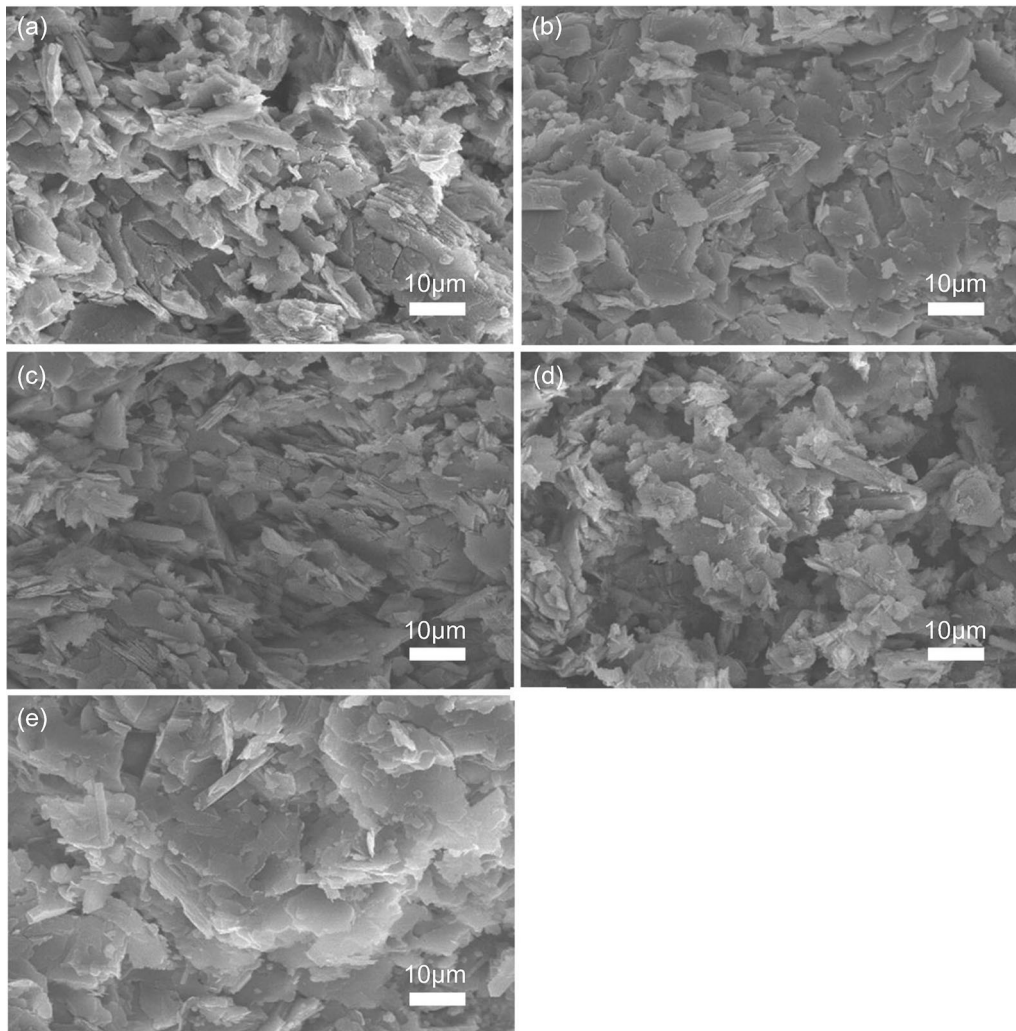**Fig. 6** Time-dependent cation concentration and pH in aqueous solution

Fig. 7 Time-dependent change in chemical composition of red-bed soft rocks samples during water saturation

Fig. 8 SEM image of microstructure of red-bed soft rocks samples over a magnification range from $3{,}000 \times$ down to 1x. **a** Before water saturation; **b** after 1 month of water saturation; **c** after 3 months of water saturation; **d** after 6 months of water saturation; **e** after 12 months of water saturation

3 Results and discussion

3.1 Time-dependent change in microscale chemical composition and pore structure in soft rock samples

Figure 6 shows that the concentrations of Na^+ and K^+ decreased exponentially with time and that the decrease was more significant during the first month after water saturation began, whereas there was little change in concentrations of Ca^+ and Mg^{2+}. Initially, concentrations of Na^+ and K^+ in aqueous solution were higher than that within the rock. This resulted in the migration of Na^+ and K^+ into the rock due to chemical potential, leading to the increase in concentration of H^+ in aqueous solution (i.e. decrease in pH). The rate of decrease in concentration of H^+ then gradually reduces until the dynamic balance of

exchange of metal ions between aqueous solution and rock is reached. The further increase in pH in aqueous solution is due to the formation of the electric double layer at the water–rock interface [26]. Figure 7 shows that there is little change in chemical composition in the red-bed soft rocks during water saturation process because a relatively small proportion of the rocks were involved in the chemical reaction.

In the process of water saturation of red-bed soft rocks, the elements of aqueous solution change and, accordingly, the element contents of rock sample should also change. It can be seen from Fig. 7 that the element contents of the rock sample do have some changes, but they are very small relative to the change of metal ion concentration in the aqueous solution. This is because the proportion of the reaction part in the total content of the soft rocks is
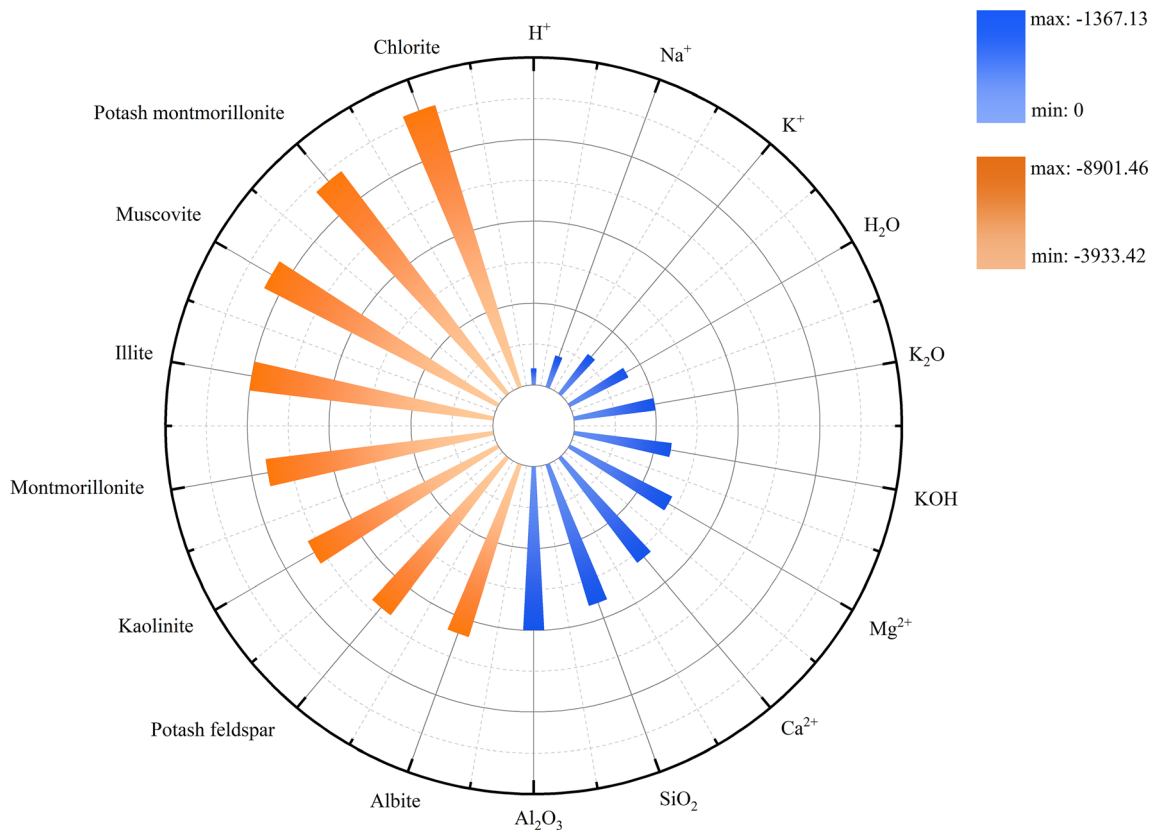
Fig. 9 The standard molar reaction enthalpy of reactants and resultant $\triangle_r H_m^0$

Table 2 Standard molar enthalpy change of related chemical reactions

Reaction sequence	Standard molar enthalpy of formation
	$\Delta_r H_m^0$ (kJ/mol)
Muscovite → albite	109.075
Potash feldspar + potash montmorillonite → kaolinite + illite	−11,332.900
Potash montmorillonite → montmorillonite	1179.656
Kaolinite → chlorite	497.540
K_2O → KOH	−193.004
Kaolinite → illite	68.170

relatively small. For the red-bed soft rocks as a whole, the percentage of element change is small.

Figure 8 shows the time-dependent change in microstructure of red-bed soft rocks before and after water saturation, quantified using SEM imaging. First, the porosity of the rock was characterised by processing SEM images through binary and the fractal box dimension. It shows that the pore structure of the rocks remained unchanged after 1 month of water saturation, although

there was a certain increase in porosity and pore expansion. After 3 months of water saturation, the connection of small pores resulted in the formation of large pores, and the shape of pores gradually changed from strip and irregular polygon to oblong and oval. After 6 months of water saturation, the total number of pores in the rock decreased, but the total area of pores increased. The shape of pores became more rounded, and the pore structure became looser. Obvious pore connection was seen after 12 months of water saturation, with significant change in the morphology of the particles due to chemical reaction. The pore shape changes flocculent and petal.

At the microscale, a series of chemical reactions took place between the minerals within the rocks and water entering fractures on the rock surface through seepage. The formation of water-soluble substances results in the loss of components of the clay mineral layer and, ultimately, changes in chemical energy. While the chemical reactions between rock minerals and aqueous solution could accelerate the damage of fracture pores, the development of factures in rock could in return promote the chemical effects. Thus, there is a close interrelation between micro-meso-macroscale chemical, physical and mechanical effects on red-bed soft rocks.

Table 3 Micro-meso-macroscale energy in red-bed soft rock samples

Rock scale	Category	Magnitude
Microscale	Adsorption energy	1.195 kJ
	Chemical energy	−44.384 kJ
	Other energy	0
Mesoscale	Potential energy	−6.390 kJ
	Swelling energy	−0.033 kJ
	Other energy	0
Macroscale	Strain energy	0.134 kJ
	Frictional energy	−0.840 kJ
	Other energy	0

3.2 Micro-meso-macroscale energy conservation during water–rock interaction

It is known that $V_{water} = 1.250 \times 10^{-2}$ m^3, $m_{sample} = 1.795$ kg, $E_{sample} = 1960$ MPa and Poisson's ratio of red-bed soft rocks $\mu = 0.280$ [66, 67]. The process of ion adsorption can be divided into surface adsorption and chemical adsorption, with an average surface adsorption of 16.732 kJ/mol and chemical adsorption of 83.720 kJ/mol [35]. Figure 9 shows the standard molar reaction enthalpy of reactants and resultant $\triangle_r H_m{}^0$ [42].

Basing on the thermodynamic parameters of reaction-related minerals and relevant thermodynamic methods [7, 40, 42], the standard molar enthalpy of formation $\Delta_r H_m{}^0$ can be obtained by using the data of standard molar enthalpy of reactants and resultants ($\Delta_r H_m{}^0 = \Delta H_{resultant} - \Delta H_{reactant}$) as shown in Table 2.

Based on the coefficients for chemical equations and the change of ion concentration before and after the process of water saturation, a polynomial equation was established with the parameters a, b, c, d, e and f, which were 0.208 mol/m^3, 0.193 mol/m^3, 0.142 mol/m^3, 0.020 mol/m^3, 0.219 mol/m^3, 0.375 mol/m^3, respectively. Therefore, the total amount of adsorbed ions in the solution (n) was 0.162 mol. Substituting the values of parameters into Eq. (7) gives

$$
\begin{aligned}
Q_{micro} &= Q_1 + Q_2 = n \cdot E_a + \sum_{i=1}^{n} c_i \cdot V_{r/w} \cdot \Delta_r H_{m_i}^0 \\
&= n \cdot E_a + c_1 \cdot V_{water} \cdot \Delta_r H_{m_1}^0 \\
&+ c_2 \cdot V_{water} \cdot \Delta_r H_{m_2}^0 + c_3 \cdot V_{water} \cdot \Delta_r H_{m_3}^0 \\
&+ c_4 \cdot V_{water} \cdot \Delta_r H_{m_4}^0 \\
&+ c_5 \cdot V_{sample} \cdot \Delta_r H_{m_5}^0 + c_6 \cdot V_{water} \\
&\cdot \Delta_r H_{m_6}^0 = -23.161 \text{ kJ}
\end{aligned}
$$

Assuming specific heat capacity c_{rock} of silty mudstone is 0.4375 kJ/(kg·°C) [11], the temperature change of red-bed soft rocks due to the exothermic reactions at microscale can be described as $\Delta T_{rock} = Q_{micro}/(c_{rock} \cdot m_{sample}) = 54.756$ °C. The above is the temperature change of soft rock mass. For the temperature change of water, it can be described as $\Delta T_{water} = Q_{micro}/(c_{water} \cdot m_{water}) = 0.441$ °C. It is consistent with the results of almost no change in the temperature of aqueous solution measured by the thermometer before and after the test. The thermal stresses $\sigma_{ft} = E_1 \cdot \varepsilon = E_1 \cdot \alpha \cdot \Delta T_{rock} = 643,930.600$ Pa, where E_1 is the elastic modulus of red-bed soft rocks, α is the coefficient of thermal expansion, $\alpha = 6 \times 10^{-6}$/°C, ε is the thermal expansion strain, and ΔT is the temperature difference of red-bed soft rocks.

Previous studies [9] showed that the initial crack length ($2c$) of red-bed soft rocks is correlated with the particle diameter of red-bed soft rocks. The average particle size of silty mudstone is about 1.500 mm [68], and the distance between adjacent cracks is about 6 mm [19]. A friction coefficient of crack surface $v = 3$, angle between the initial crack and the axial stress $\theta = 45°$, $l = \sqrt{2c} = 1.225$ mm, $P = \sigma_1 = \sigma_2 = \sigma_{ft} = 643,930.600$ Pa and $\sigma_3 = \sigma_{static} = 2450$ Pa gives

$$
F_s = \tau_f = \frac{1}{2}\mu[(\sigma_1 + \sigma_2) - (\sigma_1 - \sigma_2)\cos 2\theta] = 90.493 \text{ kPa};
$$

$$
k = (3 - \mu)/(1 + \mu) = 2.125, \quad l^{**} = 0.083c = 0.06225 \text{ mm};
$$

$$
\begin{aligned}
\tau^* &= \frac{1}{2}(\sigma_1 - \sigma_2)\sin 2\theta - \frac{1}{2}v[(\sigma_1 + \sigma_2) - (\sigma_1 - \sigma_2)\cos 2\theta] \\
&= 223.783 \text{ kPa};
\end{aligned}
$$

$$
\begin{aligned}
\sigma_{eq} &= \frac{\sqrt{2}}{2}\sqrt{(\sigma_1 - \sigma_2)^2 + (\sigma_2 - \sigma_3)^2 + (\sigma_3 - \sigma_1)^2} \\
&= 643.931 \text{ kPa};
\end{aligned}
$$

$$
\begin{aligned}
\varepsilon_{eq}^p &= \varepsilon_{eq} = \frac{\sqrt{2}}{3}\sqrt{(\varepsilon_1^p - \varepsilon_2^p)^2 + (\varepsilon_2^p - \varepsilon_3^p)^2 + (\varepsilon_3^p - \varepsilon_1^p)^2} \\
&= 2.622 \times 10^{-5}
\end{aligned}
$$

The energy change per unit surface can be assumed as 3.6 kJ/m^2 [10, 43]. At the mesolevel, the rock is composed of many particles of various sizes and cements filled between particles. To simplify the problem, the natural morphology of red-bed soft rocks is replaced by n spheres with an average particle size of 1.500 mm [34, 39, 41]. Granting to the principle of volume reciprocity, the number of particles (n) can be assumed to be 479,900–480,100 and the average value is 480 000. In addition, based on the porosity and volume changes, it can be assumed that $A_{surface} = n \cdot A_{particle} \cdot e = 1.775$ m^2 [67], where $A_{particle}$ is the surface area of particles, e is the sum of porosity and volume change rate. Further, $U^s = U^f + U^n$, where $U^f = $
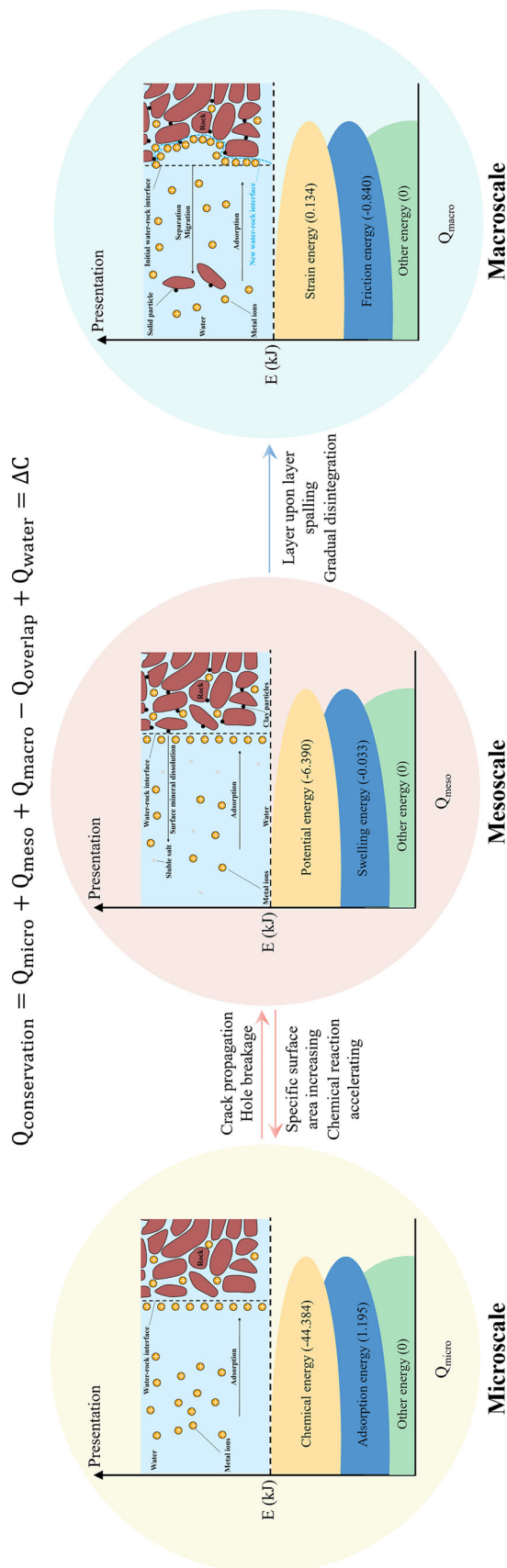
$\sum\limits_{i}^{n} \tau_f \mathrm{Al}_i$ and A is the frictional surface area. To simplify the calculation, $A = 0.008$ m^2 is calculated as twice the horizontal area of the sample, and the frictional distance $l_{i\text{-}} = 0.050$ m. The average impact force on the indirect contact surface of particles is $F_n = m_{\mathrm{particles}} \cdot g$, where $m_{\mathrm{particles}}$ is the mass of particles. The time of particle collision and friction (Δt) is calculated as 0.100 s. Thus, the micro-meso-macroscale energy can be calculated using Eqs. (7)–(15), and the results are shown in Table 3.

The adsorption of ions and chemical reactions at the microscale at the water–rock interface could lead to the increase of swelling in fracture pores at the mesoscale and an increase in change of energy in particular regions of the rock surface. While there is no overlap in microscale and mesoscale energy, the strain energy in the stress–strain curve overlaps with the potential energy at the mesoscale. Figure 10 shows the conservation of energy during water–rock interaction.

We can analyse and summarise the micro-meso-macrocorrelation mechanism of red-bed soft rocks failure within static water by energy. As shown in Figs. 10 and 11, the surface of the red-bed soft rocks specimen has a large number of microfractures and microporosity, which provides space for the movement of aqueous solution seepage. In the initial stage of soft rock encountering water, the aqueous solution enters the initial fracture and initial pore space on the surface of soft rock through seepage. At this time, the integrity of the soft rock is basically intact, and there is an obvious initial water–rock interface between the soft rock and the aqueous solution. The microscopic effect is dominated by the migration and adsorption of cations from aqueous solutions to the water–rock interface, and almost no chemical effect of clay mineral dissolution occurs. It is mainly accompanied by the adsorption energy of ions with the water absorption and swelling energy of clay minerals, etc.

As the concentration of aggregated cations within the water–rock interface becomes higher, their chemical reaction with the soft rock results in the loss of the original microstructure of the clay mineral layer. This process generates soluble salts released into aqueous solution and generates chemical thermal. The mesoscale is reflected by the crack-pore damage and the increase of surface energy. In turn, the mesoscale behaviour promotes the seepage and microchemical effects of the aqueous solution. When the clay particles continue to dissolve and fall off, it eventually leads to weakening and separation of the bond between the skeletal particles in the soft rock. This results in the formation of a new water–rock interface. At the new interface, the aqueous solution continues the above process of
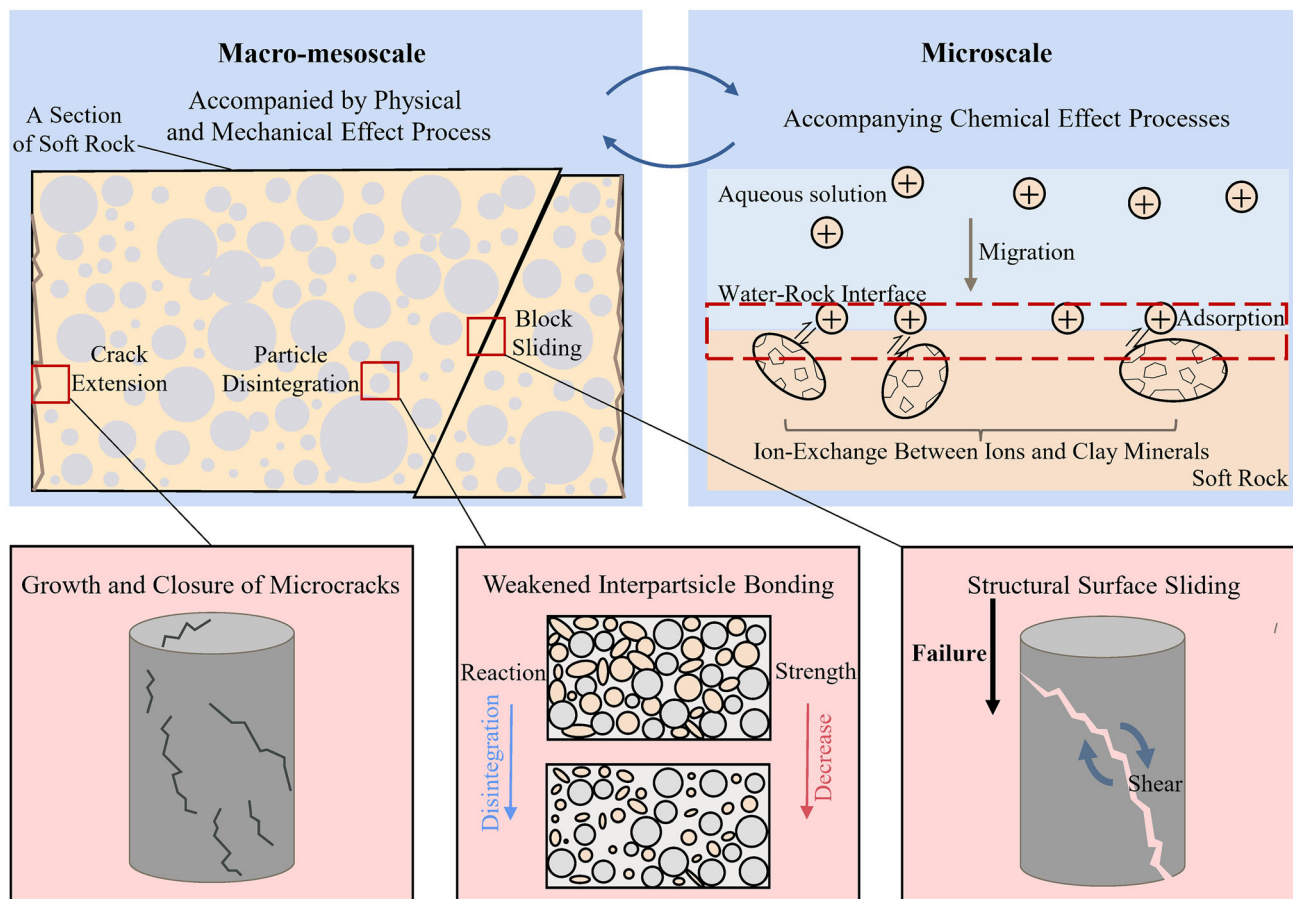

$Q_{\mathrm{conservation}} = Q_{\mathrm{micro}} + Q_{\mathrm{meso}} + Q_{\mathrm{macro}} - Q_{\mathrm{overlap}} + Q_{\mathrm{water}} = \Delta C$

Fig. 10 Micro-meso-macroscale energy conservation during water–soft rocks interaction

Fig. 11 The micro-meso-macrocorrelation mechanism of red-bed soft rocks failure within static water

seepage, dissolution and shedding of clay particles, leading to the formation of more new water–rock interfaces.

The cascade of the previous processes ultimately causes the disintegration and dislodgement of the fragments of the macroscale soft rock masses by increasing loosening. This macroscopic process is accompanied by the strain energy and the friction energy until the entire soft rock specimen is completely destroyed. The temperature in aqueous solution increases when the overall red-bed soft rocks reaction is exothermic.

As shown in Fig. 12, during the water–rock interaction, nearly 80% of the energy dissipation results from the microscale change, and meso-macroscale change accounts for the remaining 20%. Therefore, the chemical effect of the interaction between red-bed soft rocks and water is microscopic and long term. The impact on red-bed soft rock is, furthermore, the most fundamental. Thus, the chemical effects at microscale dominate the softening of red-bed soft rocks. Around 90% of the energy is generated from the chemical reaction between ions and clay minerals at the microscale, while the remaining 10% comes from ion adsorption. It can be mentioned that microscale water–rock interaction redistributes chemical elements between soft

rock and water. Chemical action is accompanied by the formation of new minerals, which will demolish the initial internal structure of the rock. At the mesoscale, the dominant potential energy (98%) leads to the damage of pores and an increase in surface area of red-bed soft rocks. As mentioned above, the change of rock microstructure under the action of water physics and chemistry constitutes the fundamental reason for the change of rock macromechanical properties. Almost all of the energy is accumulated in the red-bed soft rocks, but some of the energy releases into the aqueous solution. As shown in Fig. 13, the disintegration of the mesoparticles could appear when the energy accumulation of the mesoparticles reaches the critical point resulting in disintegration of the particles. While the damage of soft rocks fragments at macroscale results in energy dissipation, the remaining energy could be stored in the surrounding undamaged red-bed soft rocks.

Figure 14 shows that, in the early stages of water–rock interaction, water moves into rock fractures through seepage, while metal ions accumulate at the water–rock interface, resulting in ion adsorption and chemical reaction at the interface. This leads to the formation of soluble salt and mineral colloid that sheds the clay particles in the red-bed
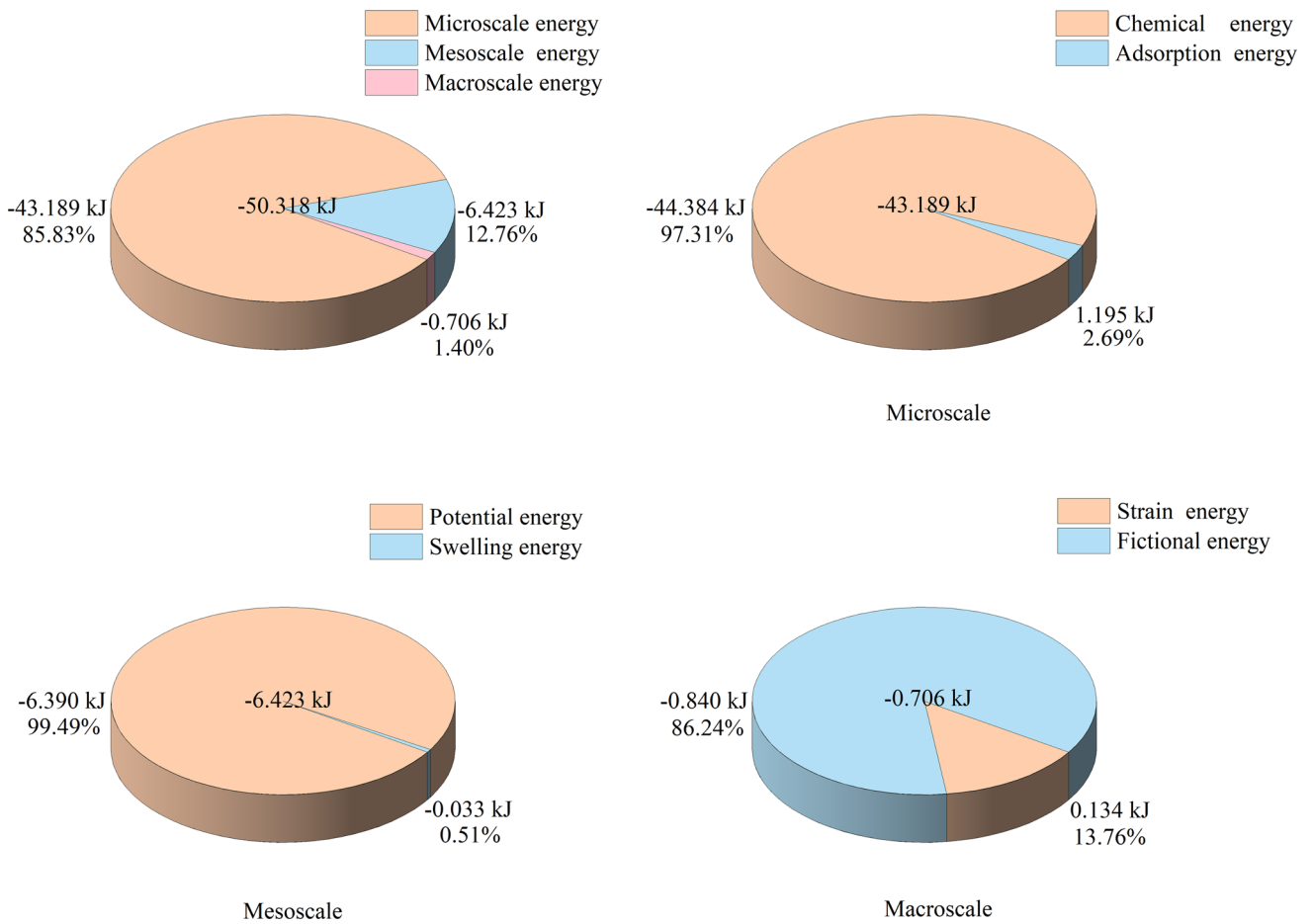
Fig. 12 Distribution of micro-meso-macroscale energy of red-bed soft rocks samples after 12 months of water–rock interaction
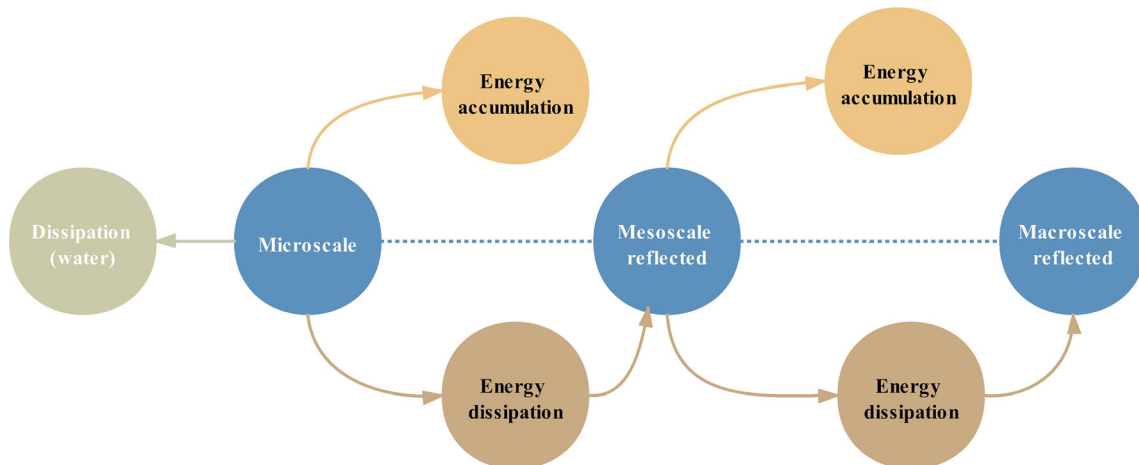

Fig. 13 Energy dissipation and accumulation at micro-meso-macroscale of red-bed soft rocks samples during water–rock interaction

soft rocks from releasing into water. Red-bed soft rocks gradually disintegrate until it was destroyed finally.

4 Conclusion

In this study, a series of experimental studies were carried out to investigate the micro-meso-macroscale correlation of red-bed soft rocks during the water–rock interaction.
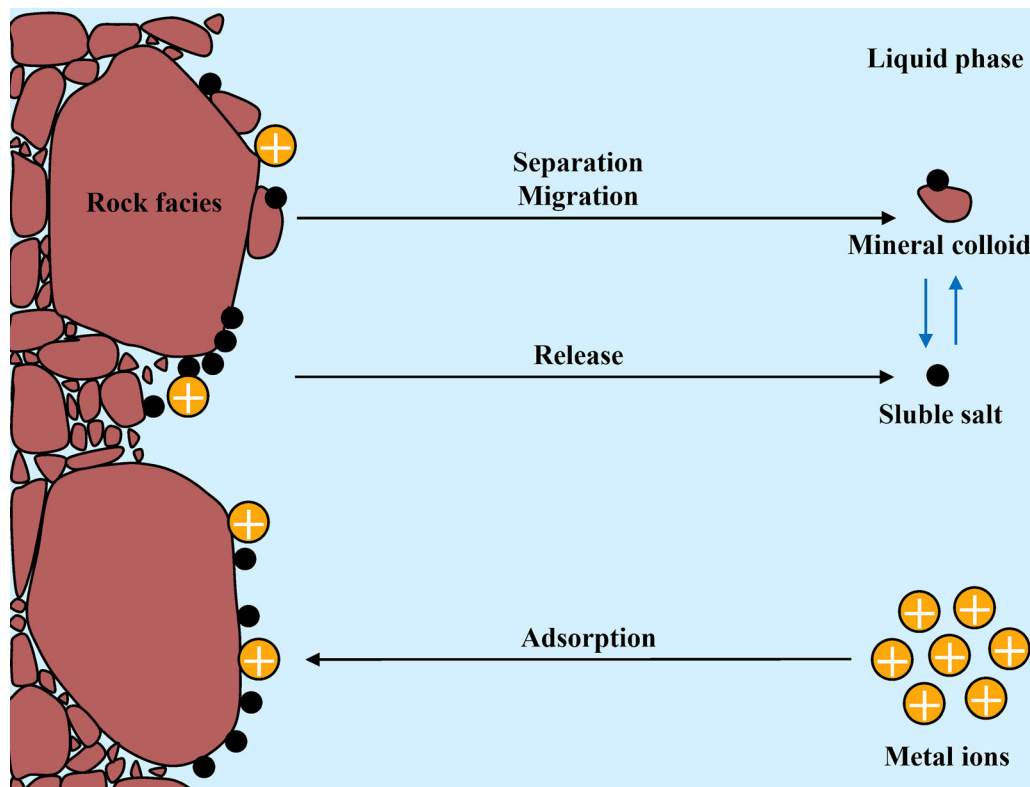
Fig. 14 Micro-meso-macroscale failure mechanism of red-bed soft rock samples during water–rock interaction

The multiscale energy conservation was also theoretically studied to understand the failure mechanism of the rocks. The following are some major conclusions:

- The microscale dominant effect of red-bed soft rocks is determined as chemical effects.
- The failure of red-bed soft rocks under water–rock interaction results from chemical, physical and mechanical dominant effects at the micro-meso-macroscale.
- The concentrations of Na^+ and K^+ in water decrease exponentially with time, and the decrease is more significant during the first month of the water saturation begins, whereas there is little change in concentrations of Ca^+ and Mg^{2+} in water.
- The transport of Na^+ and K^+ from water into rock leads to a decrease in pH in aqueous solution.
- SEM images show that change in microstructure of the red-bed soft rocks becomes obvious after 3 months of water saturation. After 6 months of water saturation, the total number of pores in the rock decreases, but the total area of pores increases.
- While there is no overlap in microscale and mesoscale energy, the strain energy in the stress–strain curve overlaps with the potential energy at the mesoscale.

- During the water–rock interaction, nearly 80% of the energy dissipation results from the microscale change, and meso-macroscale change accounts for the remaining 20%. Thus, the chemical effects at microscale dominate the softening of red-bed soft rocks.
- Around 90% of the energy generates from the chemical reaction between ions and clay minerals at microscale, while the remaining 10% is from ion adsorption.
- As a uniform measure of material evolution, energy can correlate the micro-meso-macrodominant effect of red-bed soft rock softening appropriately, which provides a new idea for revealing the catastrophic mechanism of red-bed soft rock.

Declarations

Conflict of interest The authors can confirm there are no conflicts of interest associated with this work.

Data availability statement The data used to support the findings of this study are available from the corresponding author upon request.

References

1. Arnould M (2006) Discontinuity networks in mudstones: a geological approach—implications for radioactive wastes isolation in deep geological formations in Belgium, France, Switzerland. Bull Eng Geol Env 65(4):413–422

2. Barton N (2002) Some new Q-value correlations to assist in site characterisation and tunnel design. Int J Rock Mech Min Sci 39(2):185–216

3. Barton N, Choubey V (1977) The shear strength of rock joints in theory and practice. Rock Mech (Austria) 10(1–2):1–54

4. Bian K, Liu J, Zhang W, Zheng XQ, Ni SH, Liu ZP (2019) Mechanical behavior and damage constitutive model of rock subjected to water-weakening effect and uniaxial loading. Rock Mech Rock Eng 52(1):97–106

5. Chamley H (2001) Clay Mineralogy. Encyclopedia of ocean sciences, 3rd edn. ScienceDirect, Netherlands, pp 74–81

6. Chen Z, He C, Wu D, Xu G, Yang W (2017) Fracture evolution and energy mechanism of deep-buried carbonaceous slate. Acta Geotech 12(6):1243–1260

7. Cross RJ Jr (1979) The energy requirements of a chemical reaction. Chem Phys Lett 62(3):469–472

8. Dragon A, Mroz Z (1979) A continuum model for plastic-brittle behaviour of rock and concrete. Int J Eng Sci 17(2):121–137

9. Fredrich JT, Evans B, Teng-fong W (1990) Effect of grain size on brittle and semibrittle strength: implications for micromechanical modelling of failure in compression. J Geophys Res 95(B7):10907–10920

10. Friedman M, Handin J, Alani G (1972) Fracture-surface energy of rocks. Int J Rock Mech Min Sci Geomech Abstr 9(6):757–766

11. Fuchs S, Balling N, Forster A (2015) Calculation of thermal conductivity, thermal diffusivity and specific heat capacity of sedimentary rocks using petrophysical well logs. Geophys J Int 203(3):1977–2000

12. Gurson AL (1977) Continuum theory of ductile rupture by void nucleation and growth: part I—yield criteria and flow rules for porous ductile media. J Eng Mater Technol 99(1):2–15

13. Han G, Dusseault MB (2003) Description of fluid flow around a wellbore with stress-dependent porosity and permeability. J Petrol Sci Eng 40(1–2):1–16

14. Hangzhou LI, Hongjian L, Lingwei K, Xianlun L (2007) Experimental study on stress-strain relationship of expansive mud-stone. Rock Soil Mech 28(1):107–110

15. Heggheim T, Madland MV, Risnes R, Austad T (2005) A chemical induced enhanced weakening of chalk by seawater. J Petrol Sci Eng 46(3):171–184

16. Huang BX, Li PF (2015) Experimental investigation on the basic law of the fracture spatial morphology for water pressure blasting in a drillhole under true triaxial stress. Rock Mech Rock Eng 48(4):1699–1709

17. Huang X, Liu QS, Liu B, Liu XW, Pan YC, Liu JP (2017) Experimental study on the dilatancy and fracturing behavior of soft rock under unloading conditions. Int J Civ Eng 15(6A):921–948

18. Jeong GY (2000) The dependence of localized crystallization of halloysite and kaolinite on primary minerals in the weathering profile of granite. Clays Clay Miner 48(2):196–203

19. Kemeny JM (1991) A model for non-linear rock deformation under compression due to sub-critical crack growth. Int J Rock Mech Min Sci Geomech Abstr 28(6):459–467

20. Li X, Liu Y, Tang J, Li S (2009) Dissipative particle dynamics simulation of wettability alternation phenomena in the chemical flooding process. Acta Mech Sin 25(5):583–587

21. Ling S, Wu X, Sun C, Liao X, Ren Y, Li X (2016) Experimental study of chemical damage and mechanical deterioration of black shale due to water-rock chemical action. J Exp Mech 31(4):511–524

22. Liu Z, He XF, Fan J, Zhou CY (2019) Study on the softening mechanism and control of red-bed soft rock under seawater conditions. J Mar Sci Eng 7(7):235

23. Liu JS, Jing HW, Meng B, Wang LG, Yang JJ, Zhang XF (2020) A four-element fractional creep model of weakly cemented soft rock. Bull Eng Geol Env 79(10):5569–5584

24. Liu X, Xiong L, Zhang L, Zhao M (2011) Experiment study on inhibition method of slaking properties of class-i red sandstone. J Highway Transp Res Dev 28(3):25–29

25. Liu Z, Zhou CY, Li BT, Lu YQ, Yang X (2018) A dissolution-diffusion sliding model for soft rock grains with hydro-mechanical effect. J Rock Mech Geotech Eng 10(3):457–467

26. Liu Z, Zhou CY, Li BT, Zhang LH, Liang YH (2020) Effects of grain dissolution-diffusion sliding and hydro-mechanical interaction on the creep deformation of soft rocks. Acta Geotech 15(5):1219–1229

27. Liu Z, Zhou CY, Su DL, Du ZC, Zhu FX, Zhang LH (2020) Rheological deformation behavior of soft rocks under combination of compressive pressure and water-softening effects. Geotech Test J 43(3):737–757

28. Liu Z, Zhou C, Zhu F, Zhang L (2011) Critical criterion for microstructure evolution of soft rocks in softening process. Rock Soil Mech 32(3):661–666

29. Luo DY, Su GZ, He BZ (2019) True triaxial test on rockburst of granites with different water saturations. Rock Soil Mech 40(4):1331–1340

30. Ma H, Liu QS (2017) Prediction of the peak shear strength of sandstone and mudstone joints infilled with high water-cement ratio grouts. Rock Mech Rock Eng 50(8):2021–2037

31. Mahanta B, Tripathy A, Vishal V, Singh TN, Ranjith PG (2017) Effects of strain rate on fracture toughness and energy release rate of gas shales. Eng Geol 218:39–49

32. Mogi K (1973) Rock fracture. California, USA

33. Mosser-Ruck R, Cathelineau M (2004) Experimental transformation of Na, Ca-smectite under basic conditions at 150 degrees C. Appl Clay Sci 26(1–4):259–273

34. Moyne C, Murad MA (2006) A two-scale model for coupled electro-chemo-mechanical phenomena and Onsager's reciprocity relations in expansive clays: I homogenization analysis. Transp Porous Med 62(3):333–380

35. Oelkers EH, Schott J, Devidal JL (2001) On the interpretation of closed system mineral dissolution experiments: Comment on "Mechanism of kaolinite dissolution at room temperature and pressure Part II Kinetic study" by Huertas et al. (1999). Geochimica et Cosmochimica Acta 65(23): 4429-4432

36. Ogilvie SR, Glover PWJ (2001) The petrophysical properties of deformation bands in relation to their microstructure. Earth Planet Sci Lett 193(1–2):129–142

37. Prikryl R (2001) Some microstructural aspects of strength variation in rocks. Int J Rock Mech Min Sci 38(5):671–682
38. Qi H, Feng W, Chen J, Bai H, Zhou Q (2017) The micromechanism of strength change of breccia soil in outwash deposit under rainfall at huanxipo. J Eng Geol 25(3):731–739
39. Revil A, Leroy P (2004) Constitutive equations for ionic transport in porous shales. J Geophys Res Solid Earth 109(B3)
40. Ribeiro RP, Kobelnik M, Parizotto JCV (2019) Mineralogical and thermal characterization of soft rock from Campinas, Brazil. J Therm Anal Calorim 136(2):483–492
41. Saadat M, Taheri A (2019) Modelling micro-cracking behaviour of pre-cracked granite using grain-based distinct element model. Rock Mech Rock Eng 52(11):4669–4692
42. Saxena SK (1992) Thermodynamic data. Springer, Germany
43. Shen PW, Tang HM, Wang DJ, Su XX, Huang L (2020) Weakening of mudstone fragments due to disintegration: an experimental investigation. Bull Eng Geol Env 79(10):5477–5497
44. Skiba M (2007) Clay mineral formation during podzolization in an alpine environment of the Tatra Mountains, Poland. Clays Clay Miner 55(6):618–634
45. Smith NO (1982) Elementary statistical thermodynamics. Springer, Germany
46. Souding LI, Xiao LI, Nianxue Z, Yanhui LIU (2006) Water-rock interaction of clay gouged intercalation sludging process of baota landslides in Three Gorges reservoir area. Rock Soil Mech 27(10):1841–1846
47. Steffler ED, Epstein JS, Conley EG (2003) Energy partitioning for a crack under remote shear and compression. Int J Fract 120(4):563–580
48. Su GS, Chen ZY, Ju JY, Jiang JQ (2017) Influence of temperature on the strainburst characteristics of granite under true triaxial loading conditions. Eng Geol 222:38–52
49. Tyler SW, Wheatcraft SW (1990) Fractal processes in soil water retention. Water Resour Res 26(5):1047–1054
50. Vogler D, Walsh SDC, von Rohr PR, Saar MO (2020) Simulation of rock failure modes in thermal spallation drilling. Acta Geotech 15(8):2327–2340
51. Wang X, Mu C, Gong Y, Ma D (2013) Diagenetic evolution and facies of reservoirs in Member 8 of Permian Xiashihezi formation in the Z30 block of Sulige gasfield. Acta Petrolei Sinica 34(5):883–895
52. Wei W, Huang S, Huan J (2011) Thermodynamic calculation of illite formation and its significance on research of sandstone diagenesis. Geol Sci Techol Inf 30(1):20–25
53. Wen S, Li J, Su X, Yao X (2010) Studies of mesomechanical structure characters of surrounding rock failure under complex stress state. Rock Soil Mech 31(8):2399–2406
54. Wu XY, Baud P, Wong TF (2000) Micromechanics of compressive failure and spatial evolution of anisotropic damage in Darley Dale sandstone. Int J Rock Mech Min Sci 37(1–2):143–160
55. Xie X, Chen H, Xiao X, Wang J, Zhou J (2019) Micro-structural characteristics and softening mechanism of red-bed soft rock under water-rock interaction condition. J Eng Geol 27(5):966–972
56. Yao QL, Zhang FT, Ding XL, Lei Z, Jiang G (2009) Experimental research on instability mechanism of silty mudstone roofs under action of water and its application. Proc Earth Planet Sci 1(1):402–408
57. Zhang L, Cong Y, Meng F, Wang Z, Zhang P, Gao S (2021) Energy evolution analysis and failure criteria for rock under different stress paths. Acta Geotech 16(2):569–580
58. Zhang N, Wang S, Zhao F, Li J, Sun D (2018) Review on study of interaction between soft rock and water. Water Resour Hydropower Eng 49(7):1–7
59. Zhang Y, Zeng J, Qu Z, Chen J (2015) Development characteristics and genetic mechanism of authigenic kaolinite in sandstone reservoirs of the Dongying Sag, Bohai Bay Basin. Oil Gas Geol 36(1):73–79
60. Zhao Z, Heping XIE (2008) Energy transfer and energy dissipation in rock deformation and fracture. J Sichuan Univ Eng Sci Ed 40(2):26–31
61. Zhao JX, Lu CH, Deng LM, Liu GC (2018) Impacts of simulated acid solution on the disintegration and cation release of purple rock (mudstone) in Southwest China. Geomorphology 316:35–43
62. Zhao ZH, Xie HP (2008) Energy transfer and energy dissipation in rock deformation and fracture (in Chinese). J Sichuan Univ Eng Sci Ed 40(2):26–31
63. Zheng ZS (1991) Energy transfer process during rock deformation. Sci China (Ser B) 34(1):104–117
64. Zhou CY, Huang SY, Liu Z, Lu YQ (2019) The interface process and its dynamic model of red-bed soft rock softening. Rock Soil Mech 40(8):3189–3206
65. Zhou CY, Li WK, Xiang ZM, Li JM (2015) Analysis of mesoscopic frictional contacts in soft rocks under water-stress interaction. Rock Soil Mech 36(9):2458–2466
66. Zhou CY, Liang N, Liu Z (2019) Fractal characteristics of compression failure of red soft rock and cascading failure process. Rock Soil Mech 40:21–31
67. Zhou C, Liang N, Liu Z (2020) Multifractal characteristics of pore structure of red beds soft rock at different saturations. J Eng Geol 28(1):1–9
68. Zhou C, Liu C, Liang Y, Liu Z, Wei P, Wang X (2020) Application of natural weathered red-bed soil for effective wall protection filter-cake formation. Mater Lett 258:126679
69. Zhou CY, Lu YQ, Liu Z, Zhang LH (2019) An innovative acousto-optic-sensing-based triaxial testing system for rocks. Rock Mech Rock Eng 52(9):3305–3321
70. Zhou C, Su D, Liu Z (2019) Discussion on energy dissipation mechanism in seepagechemical damage-softening process of soft rock. J Eng Geol 27(3):477–486
71. Zhou C, Yu L, You F, Liu Z, Liang Y, Zhang L (2020) Coupled seepage and stress model and experiment verification for creep behavior of soft rock. Int J Geomech 20(9):04020146
72. Zhou CY, Zhu FX (2010) An elasto-plastic damage constitutive model with double yield surfaces for saturated soft rock. Int J Rock Mech Min Sci 47(3):385–395
73. Zhou C, Zhu F, Zhang L (2010) Research on saturation test and softening critical phenomena of soft rocks. Rock Soil Mech 31(6):1709–1715
74. Zy S, Ning F (2018) Progress on the association between mesostructural parameters and macromechanical behaviors of weakly cemented rocks. Metal Mine 12:1–9